



ORIGINAL ARTICLE

Pathology of lung-specific thrombosis and inflammation in COVID-19

Rafael R. Khismatullin^{1,2} | Anastasia A. Ponomareva^{2,3} | Chandrasekaran Nagaswami¹ |
Rozalina A. Ivaeva² | Kathleen T. Montone⁴ | John W. Weisel¹  | Rustem I. Litvinov^{1,2} 

¹Department of Cell and Developmental Biology, University of Pennsylvania School of Medicine, Philadelphia, Pennsylvania, USA

²Institute of Fundamental Medicine and Biology, Kazan Federal University, Kazan, Russian Federation

³Kazan Institute of Biochemistry and Biophysics, FRC KSC of RAS, Kazan, Russian Federation

⁴Department of Pathology and Laboratory Medicine, University of Pennsylvania School of Medicine, Philadelphia, Pennsylvania, USA

Correspondence

Rustem I. Litvinov, University of Pennsylvania, 421 Curie Blvd., BRB II/III, Room 1116, 19104-6058 Philadelphia, PA, USA.
Email: litvinov@penmedicine.upenn.edu

Funding information

This research was funded by NIH grants HL148227 and HL148014, University of Pennsylvania Research Foundation grant, the Russian Science Foundation grant 21-75-00010, the Russian Foundation for Basic Research grant 19-015-00075, and the Strategic Academic Leadership Program (Priority-2030) at the Kazan Federal University.

Abstract

Background: Infection by SARS-CoV-2 produces significant pulmonary pathology including endothelial damage with resultant thrombotic events. While pathologic features were described, there are limited data on the relationship of these changes to the inflammatory response and the production of thromboses.

Objective: To investigate pathology of COVID-19-related immunothrombosis.

Patients/Methods: Tissue samples from lung, kidney, brain and heart that were collected from 45 patients who died of COVID-19. Histopathological examination was performed after H&E and Picro-Mallory staining in combination with (immuno)fluorescence to visualize neutrophil extracellular traps. Ultrastructural alterations in lungs were studied with scanning and transmission electron microscopy.

Results: Inflammatory changes and thrombosis were substantially more pronounced in the lung than in the kidney, heart, and brain. The most common pathologic finding was diffuse alveolar damage. In addition, most lung samples showed thrombi in vessels. The cause of death in single cases was massive pulmonary embolism. Ultrastructural examination revealed neutrophils attached to endothelium, perhaps as a step towards transendothelial migration. In addition, platelets were identified in the midst of fibrin as individual procoagulant balloon-like cells. Ultrastructural examination demonstrated numerous virion-like particles.

Conclusions: Studying (ultra)structural features of the autopsy lung samples from patients with COVID-19 has provided evidence for a pathogenic link between inflammation and thrombosis. The major features in the lungs of COVID-19 patients comprised primary inflammatory thrombosis associated with diffuse alveolar damage. The lungs had pronounced circulatory changes with inflammation-dependent intravascular blood clotting, whereas heart, brain, and kidneys had predominantly degenerative changes that were distinct from the lung pathology.

KEYWORDS

blood coagulation, COVID-19, inflammation, lungs, thrombosis

1 | INTRODUCTION

The disease caused by the SARS-CoV-2 virus and referred to as COVID-19 has been spread worldwide with an overall mortality rate between 1–2.3%.^{1–4} In the majority of cases, COVID-19 has prevailing respiratory clinical manifestations, ranging from mild upper airway symptoms to severe lower airway disorders, including the development of acute respiratory distress syndrome that frequently leads to respiratory failure.⁵ At the same time, COVID-19 has extrapulmonary manifestations, such as cardiac insufficiency and renal failure.^{6–8}

In addition to the relatively well-studied regional and systemic inflammation, important pathogenic mechanisms in COVID-19 are related to hemostatic disorders, underlying a prothrombotic state and life-threatening thrombotic complications.^{9,10} It has been commonly accepted that inflammation and hypercoagulability associated with endothelial dysfunction can lead to pulmonary microthrombosis.¹¹ Accumulation of neutrophils and the presence of megakaryocytes that may be native to the pulmonary tissue and produce platelets, create proinflammatory and prothrombotic conditions necessary for formation of COVID-19-associated regional intra- and extravascular clots made of platelets and fibrin.^{12,13} Although the disease severity and unfavorable outcomes are determined mainly by the acute respiratory distress syndrome, extrapulmonary organ injury and multi-organ failure has also been marked as an important predictor of mortality.¹⁴ In particular, patients with severe COVID-19 have a higher risk of kidney failure and cardiac insufficiency, both of which correlate with poor outcomes.^{6–8}

A combination of systemic inflammation and immunothrombosis has been considered one of the leading causes of death in COVID-19. However, the interplay between the inflammatory response to the SARS-CoV-2 infection and coagulopathies remain largely unclear. These complex and interrelated pathogenic reactions must include cells and mediators of innate and adaptive immunity, vessel walls and other epithelial barriers, activated platelets and clotting factors - all aimed at fighting against the viral pathogen and preventing it from invading into the blood.¹⁵

Despite the vital importance, the pathogenic mechanisms of tissue damage and structural alterations in COVID-19 are not completely understood. This study is aimed at elucidating light and ultrastructural morphological features at autopsy in patients who died of COVID-19. In this work, we studied the lung and other organs from 45 autopsies and put a special emphasis on the microthrombosis and inflammation in the lungs as the major determinant of the clinical course and outcomes of COVID-19. As a methodological advancement, we described and analyzed samples of lung tissue using multiple complementary morphological techniques, which clearly demonstrated a combination of leukocytes, multiple microthrombi and diffuse alveolar damage. In particular, we were able to show neutrophil extracellular traps using (immuno)fluorescent light microscopy and ultrastructural alterations in lungs using scanning and transmission electron microscopy. Microscopic images obtained at various resolution scales enabled us to glean new and important

ESSENTIALS

- The disease caused by the SARS-CoV-2 virus has been spread worldwide with a high mortality rate.
- The structural features of inflammation and thrombosis in various organs were analyzed with the emphasis on the lung-specific immunothrombosis.
- The pathological basis of the acute respiratory distress syndrome and a major cause of death in COVID-19 is the inflammatory thrombosis (immunothrombosis) in lungs.
- Heart, brain, and kidneys had predominantly degenerative changes and less pronounced thrombotic and inflammatory alterations that were distinct from the lung pathology.

information about the lung-specific inflammatory thrombosis and circulatory disorders that provides the structural basis for pathologic tissue alterations in COVID-19.

2 | MATERIALS AND METHODS

2.1 | Autopsy material

Complete autopsies were performed on 45 deceased patients with PCR-confirmed SARS-CoV-2 infection. All autopsies were performed at the Department of Pathology of the Clinical Hospital of the Republic of Tatarstan (Kazan, Russian Federation). The study was approved by the Ethics Committee of the Kazan (Volga region) Federal University (Resolution # 27 as of December 28, 2020). In addition, one macroscopic pulmonary thrombembolus from a research autopsy performed on a patient who died of SARS-CoV-2 infection was obtained from the Department of Pathology and Laboratory Medicine at the Hospital of the University of Pennsylvania. Clinical records of all the patients were reviewed. Tissue samples of lung, kidney, brain and heart were procured and processed for morphological examination.

2.2 | Histology

For histopathological examination, the tissue samples were fixed in 10% neutral buffered formalin, washed in water, cut into smaller pieces, then treated with in ascending concentrations of isopropanol and xylene using a tissue processor (STP420ES, Thermo Scientific), and embedded in paraffin. Four-micrometer-thick sections were stained with histological stains (H&E and Picro-Mallory histochemical kits). Twelve lung samples were used to visualize neutrophil extracellular traps (NETs), where NET-specific citrullinated histones H3 (Cit-H3) were stained using primary rabbit anti-human histone H3 antibodies (Abcam; cat. ab5103; 1:200). The samples were washed

in 0.1 M phosphate-buffered saline and incubated with secondary antibodies: donkey anti-rabbit IgG labeled with Alexa Fluor 488 (Invitrogen; A21206) for immunofluorescence staining. DAPI was used for fluorescent staining of DNA to visualize both neutrophils and NETs. Light microscopy was performed using a Zeiss AxioImager Z2 microscope.

2.3 | Scanning electron microscopy

Twelve freshly incised samples of the lung tissue or the freshly extracted pulmonary thromboembolus were rinsed with saline and fixed in an excess volume of 2% glutaraldehyde in isotonic 50 mM cacodylate buffer containing 150 mM NaCl, pH 7.4. Following fixation, the samples were cut into smaller pieces; then each of them was cut open so that the parenchymal part and the vessels could be visualized. The fixed tissues were washed in the same cacodylate buffer, then dehydrated in ascending concentrations of ethanol (30–100 v/v%), dried using hexamethyldisilazane, and sputter-coated with gold-palladium (Polaron e5100). High-resolution micrographs were obtained from randomly chosen areas of each sample to eliminate selection bias and imaged using an FEI Quanta 250FEG scanning electron microscope (FEI, Hillsboro, OR).

2.4 | Transmission electron microscopy

Four lung samples with significant inflammatory changes were initially fixed with 2.5% glutaraldehyde solution in saline (2 h) and then postfixed with 1% osmium tetroxide in 0.1 M phosphate-buffered saline, pH 7.4, for 2 h. The samples were dehydrated in ascending ethanol concentrations, acetone, propylene oxide, and embedded into Epon 812. After polymerization of the resin during 3 days at increasing temperatures from 37°C to 60°C, ultrathin sections were cut using an Ultramicrotome-III (LKB, Sweden) and stained using the standard procedure with saturated aqueous uranyl acetate and lead citrate. The specimens were examined using a Hitachi HT7700 electron microscope (Hitachi HTC, Japan).

3 | RESULTS

3.1 | Clinical information

The overall demographic and clinical characteristics of the patients involved in this study are presented in Table 1. All of the deceased patients had clinical symptoms of cardiac failure-induced pulmonary edema and subsequent fatal respiratory failure or cardiac arrest; however, the clinical causes of death varied among patients. In accordance with the guidelines issued by the Ministry of Public Health of the Russian Federation,¹⁶ all the patients enrolled in this study received standard treatment, including immunosuppressive medications and low molecular weight heparin.

TABLE 1 Characteristics of the deceased patients with COVID-19 enrolled in this study

Clinical and demographic data	Patients (n = 45)
Average age, years	72 ± 12
Sex (female)	27 (60%)
Complications and comorbidities	
Hypertension	43 (96%)
Renal failure	38 (84%)
Ischemic heart disease	25 (56%)
Obesity	19 (42%)
Bacterial pneumonia	12 (27%)
Pulmonary macrothrombosis	7 (16%)
Diabetes mellitus	7 (16%)
Pulmonary embolism	4 (9%)
Clinical causes of death	
Respiratory failure, pneumonia	36 (80%)
Sudden cardiac death	5 (11%)
Cardiorespiratory failure, pulmonary embolism	4 (9%)

3.2 | Pathologic alterations in the lungs

3.2.1 | Macroscopic alterations, histology and immunohistochemistry

In all patients, postmortem examination revealed that the lungs were heavy (>700 g) compared to normal lung weights (350–450 g) and congested. The lung surface often had a distinct patchy structure with dense dark reddish hypervascular areas alternating with pale softer zones. The lungs were characterized by the outflow of a large amount of pink foaming fluid upon incision, which corresponded to abundant intra-alveolar microscopic tissue edema.

Histologically, in the vast majority of the samples (87%), multiple microthrombi in capillaries (Figure 1A) and larger primary thrombi in arterioles (Figure 1B) were present. These thrombi were considered to be primary in nature as there was no evidence for venous occlusion of the lower limbs and pelvic floor at autopsy and no premortem clinical records indicating deep vein thrombosis. In only 9% of cases, the cause of death was a massive pulmonary embolism that included a large embolus in the trunk as well as emboli in small branches of the pulmonary artery (Table 1). In these patients, formation of these multiple large and small pulmonary emboli was associated with the clinically diagnosed deep vein thrombosis and/or thrombosis of the right chamber of the heart. In these thromboemboli that were 10–13 mm in diameter, fibrin was accumulated at the periphery and the adjacent lung tissue was infiltrated with leukocytes, mainly mononuclear cells. The internal structure of pulmonary emboli showed alternation of fibrin and erythrocyte layers, with a significant predominance of erythrocytes. It is noteworthy that fibrin in pulmonary emboli was a few

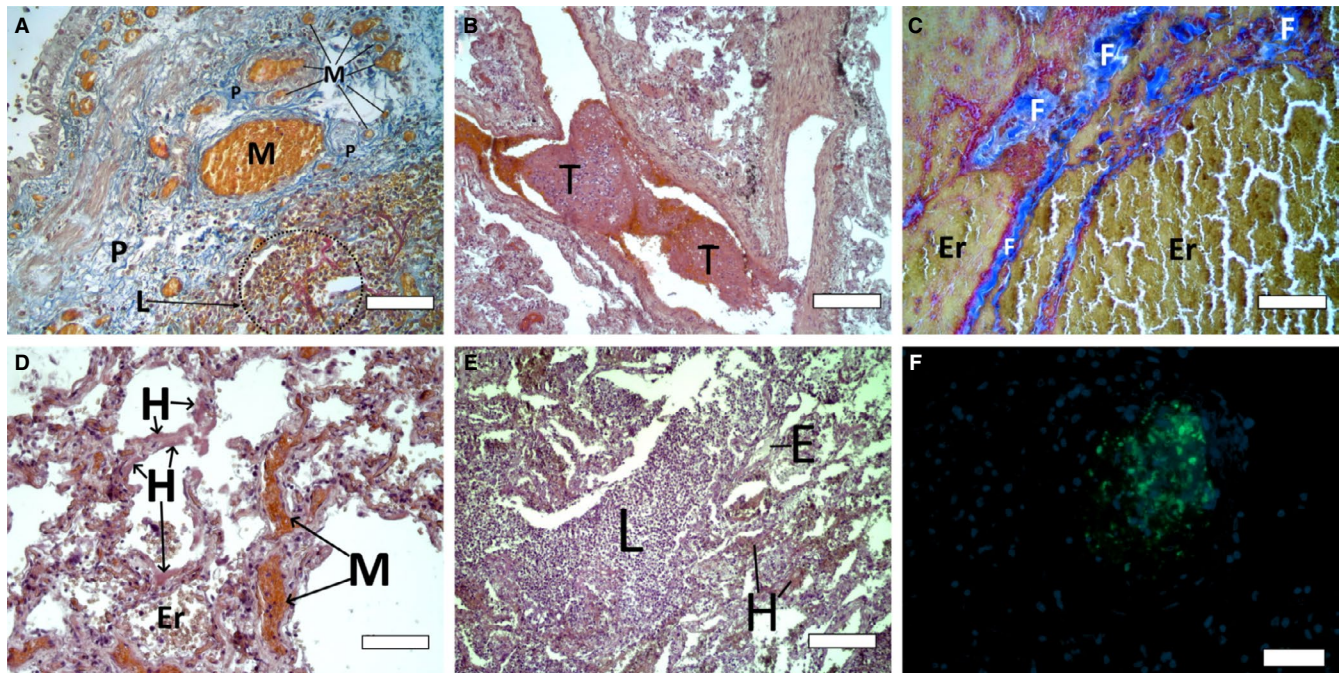


FIGURE 1 Representative histological images showing characteristic structural alterations in the autopsy lung tissue samples from patients who died of COVID-19. (A) Multiple microthrombi (M) consisting mainly of erythrocytes; focal pneumofibrosis and perivascular fibrosis (P); and leukocyte infiltration (L). Picro-Mallory stain, magnification bar =100 μ m. (B) Thrombi (T) attached to the vessel walls and containing predominantly fibrin and leukocytes. H&E, magnification bar =200 μ m. (C) Internal structure of a pulmonary thrombotic embolus with alternation of the blue (old) fibrin (F) and erythrocyte (Er) layers. Picro-Mallory stain, magnification bar =100 μ m. (D) Alveoli with microthrombi (M), diapedesis of single erythrocytes (Er), and hyaline membranes (H). H&E, magnification bar =50 μ m. (E) Infiltration of lung tissue with neutrophils (L), focal edema (E) and hemorrhage (H). H&E, magnification bar =100 μ m. (F) Blood vessels containing microthrombi stained for histones CitH3 (green) and DNA (blue) to visualize neutrophils and NETs. The surrounding extravascular cells are DAPI-positive (blue) due to the presence of DNA. Fluorescence, magnification bar =100 μ m

days or more old, as indicated by the blue color with the Picro-Mallory stain (Figure 1C), suggesting that clots formed at least 24 h before they were removed and fixed.¹⁷

In addition to microthrombosis, the most common histological findings in the lungs were inflammatory cells (in 80% of samples), distinct hyaline membranes (73%), capillary congestion and blood stasis detected as vasodilation combined with increased content of blood elements in the microvasculature (60%), hemorrhage (82%) and interstitial edema (100%). Numerous samples of lungs showed diffuse alveolar damage (Figure 1D). Some lungs had no significant diffuse alveolar damage, but rather extensive neutrophilic infiltration resembling bacterial bronchopneumonia (27%) (Figure 1E). As a valid sign of inflammation, accumulation of neutrophils and neutrophil extracellular traps (NETs) associated with thrombosis were clearly detected in the vascular lumens (Figure 1F), using (immuno) fluorescence of NET-specific citrullinated histones H3 and DNA. Notably, the NETs were associated with intravital clinical manifestations of severe inflammation, including tachycardia, tachypnea, and high fever.

In addition to the alterations related to the acute COVID-19, long-term or chronic pulmonary pathological changes were frequently observed, such as destruction of alveolar septae (100%) and focal lymphocytic infiltration of the bronchi (11%), likely associated with pre-existing conditions and comorbidities.

3.2.2 | Ultrastructural alterations

Scanning and transmission electron microscopy revealed detailed structural alterations in the COVID-19 lungs at a much higher level of spatial resolution. Presumable fibrin masses recognized as amorphous proteinaceous depositions on septal membranes were the most abundant structure on the surface of the alveolar septa, which may correspond to the histologically revealed hyaline membranes, the main microscopic feature of diffuse alveolar damage (Figure 2A). These extremely dense agglomerates of fibrin, dead cells, and surfactant¹⁸ were characterized by close adherence to the septa and lack of porosity. There were also other morphologic types of fibrin, yet present in a much smaller amount. Structurally, they were less dense and sparser than those described above and had a fibrillar (fibers and bundles) or spongy structure; they were freely located in the lumens of the alveoli, not attached or tightly adherent to the alveolar septa (Figure 2B).

The blood vessels were dilated and contained blood cells, mainly erythrocytes (Figure 2C). The endothelial cells of the inner vascular wall were often flattened. In 83% of samples, blood cells were found in a similar quantity both inside the vessels and in the lumen of alveoli; however, within the vessels, erythrocytes were tightly packed, which is a sign of microthrombosis. It is noteworthy that compressed and deformed erythrocytes often adhered tightly to the inner wall

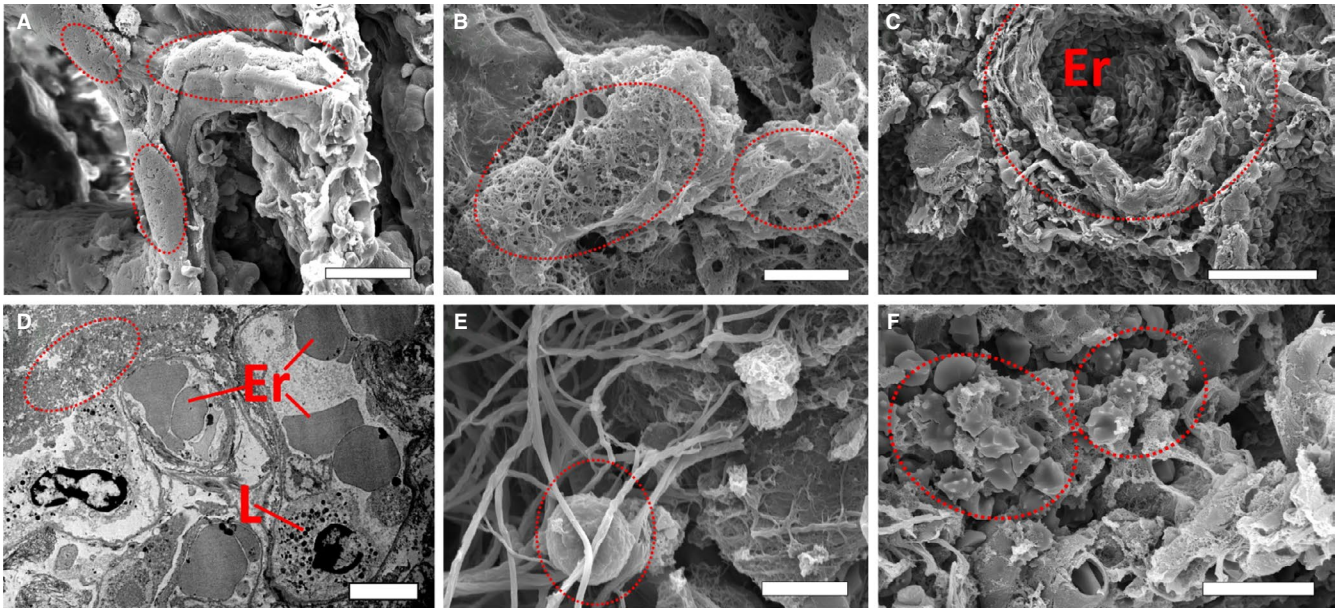


FIGURE 2 Representative electron microscopy images showing characteristic structural alterations in the lung tissue samples from patients who died of COVID-19. (A) A scanning electron micrograph of compacted non-porous depositions of fibrin, dead cells and surfactant (*dotted ovals*) attached to the alveolar septa. Magnification bar =25 μm . (B) A scanning electron microscopy image of a spongy fibrous fibrin-like structure (*dotted oval*) in the lumen of alveoli, not attached or tightly adherent to the alveolar septa. Magnification bar =5 μm . (C) A scanning electron micrograph showing the lumen of a dilated blood vessel (*within the dotted circle*) containing sparse and compacted blood cells, mainly erythrocytes (*Er*). Magnification bar =50 μm . (D) Transmission electron microscopy of capillary lumens with irregularly shaped (compressed) erythrocytes (*Er*) and leukocytes (*L*) inside. Destroyed vessel walls as well as the surrounding cells and tissues are shown (*dotted oval*). Collagen fibers and edematous tissue are seen behind the basement membrane. Magnification bar =5 μm . (E) Scanning electron microscopy showing individual balloon-like platelets (*within the dotted oval*) among fibrin fibers. Magnification bar =5 μm . (F) Echinocytes (*within the dotted ovals*) in the extravascular space. Magnification bar =15 μm

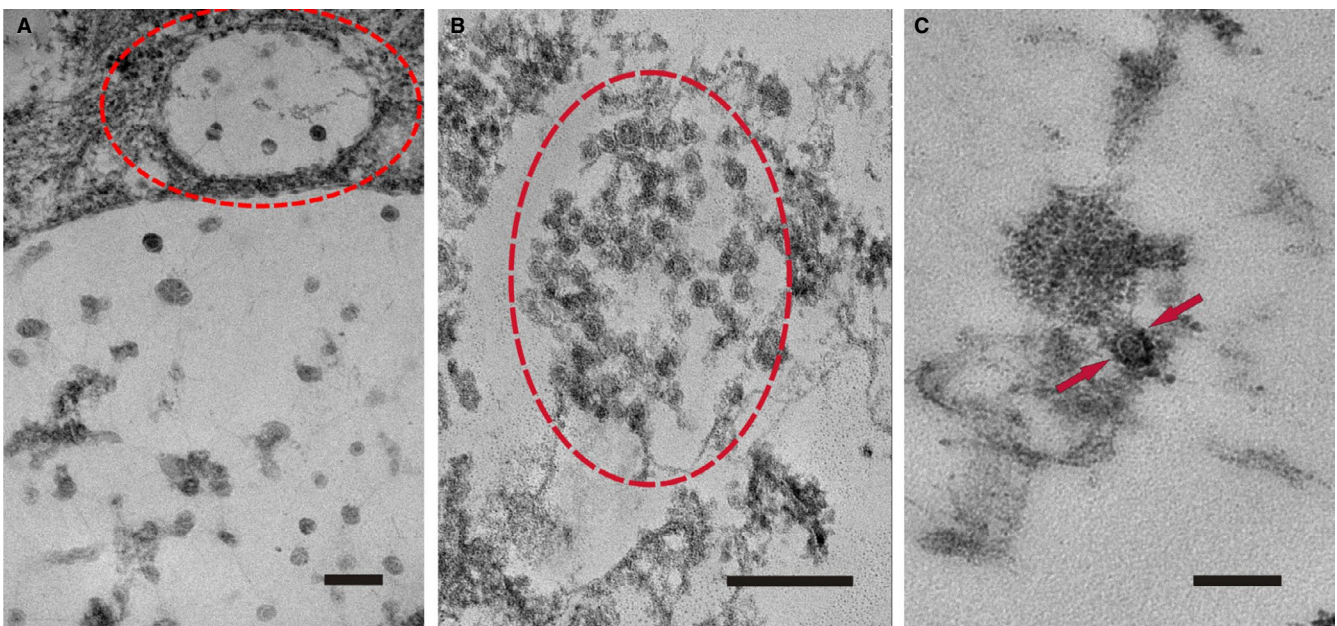
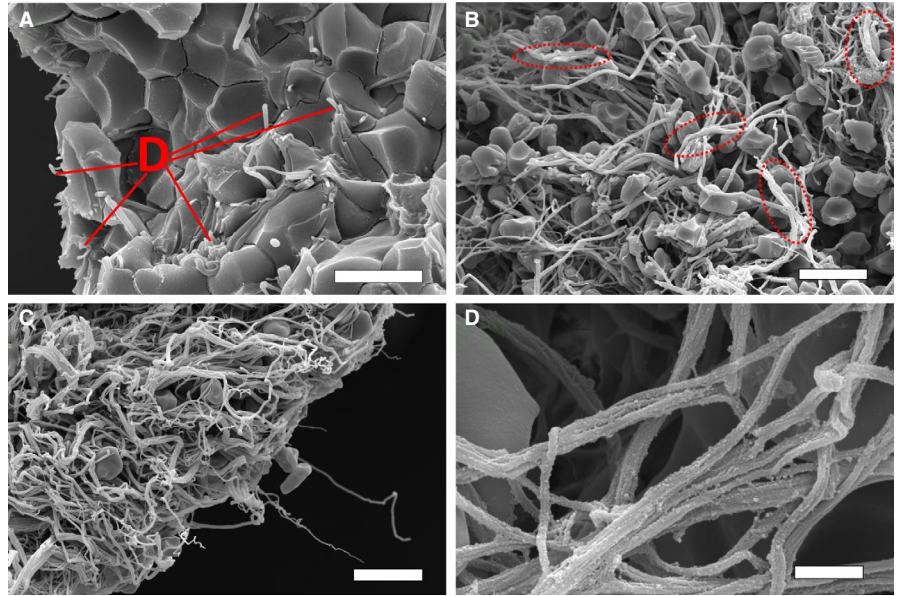


FIGURE 3 Representative high-resolution transmission electron microscopy images of coronavirus-like particles in the lung tissue of a patient who died of COVID-19. (A) Small (*lined oval*) and large (*below*) membrane-bound vacuoles containing particles within the cytoplasm of a type II pneumocyte. (B) A cluster of extracellular virion-like particles (*lined oval*) in the alveolar space. (C) An extracellular particle with distinctive spike-like projections (shown by *arrows*). Magnification bars =200 nm

FIGURE 4 Representative scanning electron microscopy images of a pulmonary blood clot from a patient who died of COVID-19. (A) Compacted polyhydrocytes and a small amount of free barbed fibrin fiber ends (E). Magnification bar =5 μm . (B) Fibrin bundles (dotted ovals) and fibers in the clot. Magnification bar =10 μm . (C) The peripheral part of the clot containing a large amount of fibrin. Magnification bar =10 μm . (D) Fibrin bundles coated with sparse spherical microparticles. Magnification bar =1 μm



of blood vessels, and the cellular part of a microthrombus was often separated from its proteinaceous portion (fibrin).

In 83% of the lung samples examined, leukocytes were found both within and outside the blood vessels. In the scanning electron microscopy images, they could be identified as the largest blood cells with a rough surface. Using high-resolution transmission electron microscopy, the type of white blood cells could be specified. In some samples, neutrophilic leukocytes were attached to the endothelium, indicating ongoing active exudation. A relatively small fraction of leukocytes was represented by mononuclear cells, both lymphocytes and monocytes, but the vast majority of leukocytes were neutrophils, which corresponded to the histological findings previously demonstrated in Figure 1E.

All erythrocytes within microthrombi could be segregated into several morphological types: (i) uncompressed pure biconcave cells, (ii) partially or fully compressed cells as a result of mechanical clot compaction (namely, intermediate mainly biconcave, mainly polyhedral and polyhedral) (Figure 2D) and (iii) echinocytes that comprise metabolically altered erythrocytes formed over time as a result of hypoxia. Platelets inside thrombi sometimes could be identified as individual balloon-like cells (Figure 2E), resulting from osmotic inflation; however, no individual discoid-like platelets, platelet aggregates or megakaryocytes could be found. Outside thrombi and in the extravascular space, echinocytes were observed frequently (Figure 2F), while they were uncommon within the microthrombi.

Signs of alveolar cell destruction were clearly visible and common. Some alveocytes displayed signs of necrosis, such that the cytoplasm disintegrated into lumps (plasmorexis) and the nucleus disappeared (karyolysis). There were multiple tears of the interalveolar septa manifesting as exposure and damage of fibrous structures (collagen) and desquamation of alveocytes into the lumen of the alveoli. Most of the lung tissue demonstrated signs of atelectasis.

3.2.3 | Visualization of virion-like particles

In 33% of the lung samples analyzed with scanning electron microscopy, many spherical particles 100 ± 50 nm in diameter, likely representing the SARS-CoV-2 virions, were found on the surface of various structural elements, including alveocytes and blood cells. High-resolution transmission electron microscopy of a lung sample from a deceased patient with PCR-confirmed SARS-CoV-2 infection revealed multiple virion-like microparticles with distinctive prominent surface projections. The diameters of the virion-like particles varied from 30 nm to 67 nm with an average diameter of 49.8 ± 10.0 nm ($n = 60$). The particles could be visualized inside the intracellular vacuoles of type II alveolar epithelial cells (Figure 3A), but they were often found in the extracellular space, either as sparse structures or large clusters (Figure 3B). Most of the virion-like particles had distinct boundaries and a dense internal matrix. Figure 3C shows a single virion-like particle with clearly seen protrusions on the surface; the size of the particle body was 60 nm, while with the spike-like frame it reached 100 nm (Figure 3C).

3.2.4 | Structure and composition of a large pulmonary blood clot

The overall structure and composition of a large pulmonary blood clot were analyzed using 48 scanning electron micrographs obtained from randomly selected areas. Erythrocytes comprised the major volume fraction of the clot and prevailed over fibrin. Empty spaces or intercellular pores occupied an insignificant portion of the clot volume, indicating that this clot was quite compact and hardly permeable. Erythrocytes were the prevailing type of blood cells in the clot. Deformed erythrocytes, originating from platelet-driven contraction and compression of

the clot, included polyhedrocytes (median volume fraction 82%, IQR 55; 90), intermediate mainly polyhedral cells (15%, IQR 6.8; 28), and slightly deformed erythrocytes with mainly biconcave shape (3.5%, IQR 0; 13.8) (Figure 4A). In addition, single biconcave erythrocytes, spherocytes, and echinocytes could be identified. It should be noted that the shape of the cells, the density of their packing and arrangement were approximately the same throughout the clot and did not depend on whether they were in the center or at the periphery of the clot. The prevalence of compressed deformed erythrocytes indicates marked intravital contraction of the clot.

Fibrin was the second most abundant structural element in the clot. Three main morphological types of fibrin structures were revealed, namely individual fibers, bundle fibers, and fibrin remnants (debris) with barbed free ends that likely originated from proteolytic cleavage. Fibrin bundles and long fibers prevailed significantly over truncated fibers with free ends (Figure 4B). Fibrin was present through the clot, while fibers with free ends were located mainly at the clot periphery and extended outside (Figure 4C), suggesting external proteolysis. Remarkably, some fibrin fibers were coated with small spherical microparticles approximately 50–100 nm in size (Figure 4D), which could comprise virions or cellular ectosomes indistinguishable by size.¹⁹

3.3 | Pathological alterations in the cardiac tissue

Morphological signs of thrombotic and circulatory disorders in the cardiac vessels were less common compared to the lungs and had distinct histological features. Macrothrombi were observed in only 13% of the samples and microthrombi were found in 24% of the cardiac samples analyzed. In one patient, a thrombus was found in the cavity of the right atrial appendage, which was the source of pulmonary embolism (Figure 5A). The prevailing pathological features in the heart samples were manifestations of chronic pre-existing conditions, including high-grade coronary artery sclerosis (89% samples), myocardial scarring (20%), and venous plethora (49%), indicating ischemic heart disease and/or ischemic cardiomyopathy. Acute focal degeneration of cardiomyocytes, a manifestation of systemic circulatory disorders not related to occlusion of coronary arteries, was observed in the vast majority of samples (84%) (Figure 5B). No histological signs of inflammation were revealed in the cardiac tissue.

3.4 | Pathological alterations in the brain tissue

Histologically, microthrombosis of cerebral vessels was observed in about 47% of the samples analyzed. In all the samples, without exception, the brain tissue had signs of significant pericellular and

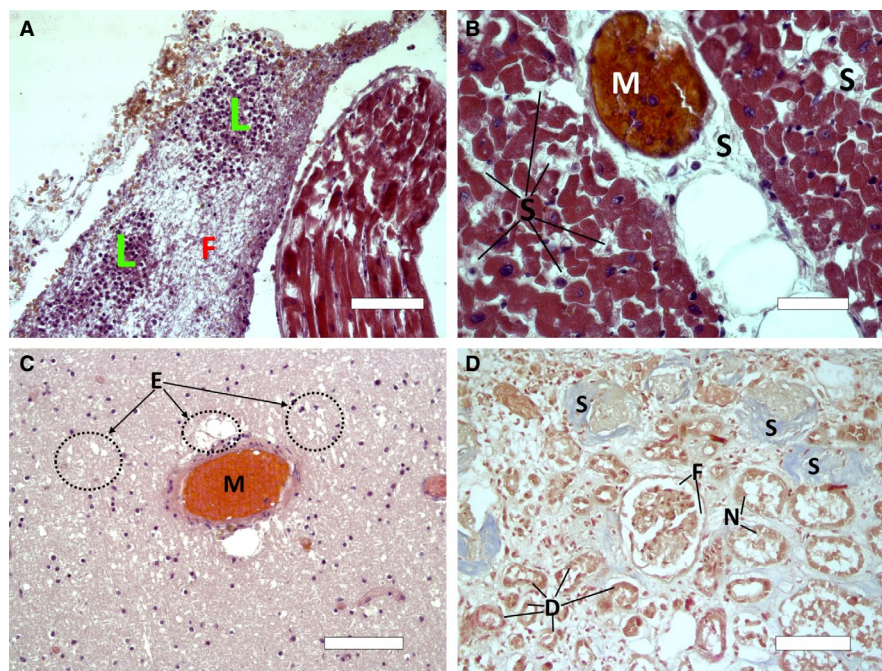


FIGURE 5 Representative histological images, showing characteristic structural alterations of the autopsy samples of heart (A, B), brain (C) and kidney (D) from patients who died of COVID-19. (A) A heart cavity with a thrombus composed mainly of fibrin (F) and neutrophilic leukocytes (L). H&E, magnification bar =100 μ m. (B) Microthrombi (M) in a vascular lumen; extensive sclerosis of the coronary arteries and cardiosclerosis (S), degeneration of cardiomyocytes. H&E, magnification bar =50 μ m. (C) A microscopic thrombus (M) composed mainly of erythrocytes; pericellular and perivascular edema of brain tissue (E). H&E, magnification bar =100 μ m. (D) Acute tubular necrosis appearing as the absence of nuclei in the cells of tubules (N); parenchymatous focal degeneration of tubular epithelium (D); glomerulosclerosis (S); and fibrin deposits (F) in a Bowman's capsule. Picro-Mallory stain, magnification bar =100 μ m

perivascular edema (Figure 5C). There were no other significant and consistent changes revealed in the brain tissue.

3.5 | Pathological alterations in kidneys

In all the samples analyzed, there were histological signs of acute tubular injury, mainly in the proximal tubules. This injury included tubular necrosis (in 82% of samples) and/or degeneration (100%) that manifested as the vacuolar degeneration and detachment of epithelial cells with barely discernible tubular basement membrane (Figure 5D). The dilation of the tubular lumen with cellular debris as well as the loss of brush border was revealed consistently. Distal tubules and collecting ducts had occasional edematous expansion of the interstitium with no signs of inflammation.

Hyalinosis of arterioles and arteriosclerosis of the medium-size arteries in glomeruli were revealed in 53% of the samples and likely corresponded to chronic nephropathy, typical for diabetes or arterial hypertension. Signs of ischemia with accumulation of fibrin in the Bowman's space and shrinkage of capillary loops were present in 22% of the kidney samples.

4 | DISCUSSION

To reveal COVID-19-related pathological changes, we examined autopsy samples of lung, heart, kidney and brain tissues from patients who died of COVID-19, with the emphasis on the lungs as the main target of SARS-CoV-2 infection. Despite the extensive literature on postmortem pathological data in COVID-19, the pathophysiology of this disease is still not fully understood, and new autopsy findings provide a fundamental structural basis to gain insights into the pathogenic mechanisms that lead to lethal outcomes, as has been demonstrated for other infectious diseases.^{20,21} Although most studies have focused on the pronounced pulmonary alterations, a few papers have demonstrated alterations of other organ systems in fatal COVID-19 infections.^{22,23} There is strong evidence that SARS-CoV-2 causes systemic endothelial dysfunction,²⁴ which is responsible for the multi-organ dysfunction and failure.²⁵ Here, we compared the structural features of various organs with the focus on thrombosis and inflammation in the lungs. It was shown in earlier studies that the most important feature of COVID-19 is regional microthrombosis of the lung vessels, alongside the relatively high prevalence of deep vein thrombosis and subsequent pulmonary embolism.^{25,26} Our findings generally confirm these observations, but on an extensive cohort of patients and with addition of important structural details on the pathology of inflammation and thrombosis in the lungs in patients who died of COVID-19. The results obtained strongly support the important role of inflammatory cells in the development of lung-specific immunothrombosis. To advance the methodology of postmortem morphological analysis, in our study histopathological examination in combination with (immuno)fluorescence was complemented with scanning and transmission electron microscopy to

gain high-resolution structural information about the pathologic structural pulmonary and extrapulmonary alterations in COVID-19. All this allowed us, in contrast to many previous investigations, to obtain an extremely detailed and comprehensive morphological description of ultrastructural tissue lesions, as well as to visualize NETs and virion-like particles.

Inflammation and thrombosis were substantially more pronounced in the lungs than in kidneys, heart, and brain, in which we observed only degenerative and minor circulatory changes (Table 2), which is consistent with other studies.²⁷ The most common morphological signs of tissue damage in the lungs comprised alveolar destruction (often manifested as diffuse alveolar damage) with pulmonary edema, which corresponds to clinically observed respiratory failure (Figures 1D and 2A). Strictly speaking, these pathological alterations could be not fully related to the inflammatory lung injury. Given the older age of the deceased patients and the presence of comorbidities (hypertension, obesity, type II diabetes) (Table 1), the edema itself could be caused and aggravated by a combination of pulmonary and extrapulmonary causes. The acute pneumonitis, pulmonary thrombotic embolism, and regional thrombosis of the lung microvasculature were often combined with ischemic heart disease, cardiomegaly, and sepsis that could exaggerate the respiratory problems. Irrespective of the underlying pathogenic mechanisms, respiratory failure was the ultimate cause of death in all of the patients analyzed.

There is a controversy in the literature as to whether the COVID-19-related micro- and macrothrombi in lungs are formed primarily *in situ* or they comprise secondary thrombotic emboli originating from an extrapulmonary thrombus.¹¹ In the vast majority of the samples analyzed here, the thrombotic obstruction of lung vessels associated with acute inflammation was observed in the absence of detected deep vein thrombosis, which is an argument for primary microthrombosis in the lungs, rather than pulmonary embolism.²⁸ Other authors have also found that pulmonary microthrombi in COVID-19 are due to the local hypercoagulability and are not originating from thrombi of the lower extremities.^{29,30} However, in a few cases we observed a typical secondary pulmonary embolus in a COVID-19 patient (Tables 1 and 2, Figure 1C). Given a high risk of deep vein thrombosis in COVID-19,³¹⁻³³ pulmonary thrombotic embolism is highly likely and can further exaggerate the respiratory dysfunction. As for the large pulmonary clot presented in Figure 4, based on the absence of clinical and autopsy data for deep vein thrombosis and strong contraction, which is not typical for thrombotic emboli,³⁴ this is a primary thrombus rather than an embolus. Therefore, in COVID-19 the primary pulmonary thrombosis and thrombotic embolism in the lung artery and/or its branches seem probable, but with a prevalence of the primary immunothrombosis.

Diffuse alveolar damage with the formation of impermeable hyaline membranes combined with inflammation is primarily responsible for the gas exchange disorders in COVID-19 and comprises the hallmark of acute respiratory distress syndrome.^{18,35} The morphological pattern of COVID-19-related pneumonitis becomes apparent predominantly as an inflammatory vascular injury with significant fibrin

Morphological features	Incidence (Total n = 45)	Causative relation to COVID-19
Lung		
Destruction of alveolar septa	45 (100%)	Definitely
Edema	45 (100%)	Highly likely
Microthrombi	39 (87%)	Definitely
Hemorrhage	37 (82%)	Definitely
Leukocytes	36 (80%)	Definitely
Fibrin deposits in alveoli ("hyaline membranes")	33 (73%)	Definitely
Stasis of blood	27 (60%)	Highly likely
Thrombi in arterioles	7 (16%)	Definitely
Microparticles (SEM, n = 12; TEM n = 4)	4 (33%)	Definitely
Thrombotic emboli	4 (9%)	Highly likely
Neutrophil extracellular traps (NETs) (IHC, n = 12)	1 (8%)	Definitely
Heart		
Coronary artery sclerosis	40 (89%)	Unlikely
Degeneration of cardiomyocytes	38 (84%)	Likely
Venous plethora	22 (49%)	Likely
Microthrombi	11 (24%)	Highly likely
Myocardial scarring	9 (20%)	Unlikely
Thrombus in a vessel	6 (13%)	Highly likely
Thrombus in the heart cavity	3 (7%)	Likely
Brain		
Edema	42 (93%)	Likely
Microthrombi	21 (47%)	Highly likely
Kidney		
Degeneration of tubular epithelium	45 (100%)	Likely
Acute tubular necrosis	37 (82%)	Highly likely
Sclerosis of glomeruli	24 (53%)	Unlikely
Fibrin deposits in glomeruli	10 (22%)	Likely

TABLE 2 Structural alterations and their frequency in the autopsy tissue samples from patients who died of COVID-19

deposition (on septal walls and within alveolar lumens) as well as alveolar infiltration with neutrophils (Figure 1E). The multiple fibrillar and spongy structures could comprise a mixture of fibrin and NETs because discrimination between fibrin and NETs by scanning electron microscopy is hardly feasible.³⁶

Because neutrophils are the most abundant cells in the lungs of COVID-19 patients, they are the source of NETs formed at the sites of inflammation (Figure 1F). NETs have been shown to promote fibrin deposition, platelet activation, disturb the local blood flow, and reduce the susceptibility of thrombi and microthrombi to fibrinolysis and to therapeutic thrombolysis.^{37,38} This processes leads to inflammation-dependent intravascular blood clotting or immunothrombosis^{39,40} that exacerbates tissue injury by triggering and promoting vessel occlusion and hypoxia.⁴¹ NETs and microthrombi form a positive feedback loop and together can worsen the respiratory insufficiency in COVID-19 due to profound disturbance of the lung microcirculation. These alterations may include extravasation of

neutrophils with subsequent inflammatory damage of the surrounding lung tissue (Figures 1A,D,E and 2A,D). Endothelial activation and accumulation of von Willebrand factor at the site of microthrombosis also contribute to impaired blood circulation and gas exchange in the lungs.⁴² This is in line with the ability of NETs to cause cellular death of the lung epithelium,⁴³ thereby aggravating the disease. The aggregate of data suggests that modification of NET formation and their composition could represent a potential therapeutic approach in COVID-19 and perhaps other inflammatory and infectious diseases.⁴⁴

The morphology of the virion-like particles revealed with scanning and transmission electron microscopy (Figure 3) is generally consistent with the ultrastructure of SARS-CoV-2 virions observed in tissues of COVID-19 patients,⁴⁵⁻⁴⁷ including the cells of the respiratory tract.⁴⁸ However, without specific identification, we prefer calling them "coronavirus-like" structures, as suggested by others.^{47,49} Importantly, the observed virion-like particles were revealed

inside vacuoles in the cytoplasm of type II pneumocytes as well as in the extracellular space, perhaps formed as a result of inflammatory cellular destruction.

All of the structural pathological features described underlie not only the lung injury and respiratory failure, but also the disease progression in the form of multi-organ injury, including degeneration of extra-pulmonary tissues^{47,50} and a high risk of micro- and macrovascular thrombotic complications in COVID-19.⁵¹

5 | CONCLUSIONS

To get insights into the pathology of COVID-19, the structural features of inflammation and thrombosis in various organs were analyzed with the emphasis on the lung-specific immunothrombosis. Based on histological examination, immunohistochemistry, and electron microscopy of the autopsy tissues of patients with clinically proven fatal cases of COVID-19, the most important and characteristic pathological features comprise the profound lung damage that includes diffuse inflammatory (micro)thrombosis, widespread alveolar damage, and pronounced inflammation manifested as immune cell infiltration and formation of NETs. Heart, brain, and kidneys had relatively minor morphological signs of injury and circulatory disorders that indicated their involvement in the pathogenesis of COVID-19 but to a lesser extent. The pathological findings matched clinical manifestations of the disease and provided a structural basis for the severe course and fatal outcomes of COVID-19. To summarize, the pathological basis of the acute respiratory distress syndrome and a major cause of death in COVID-19 is the inflammatory thrombosis (immunothrombosis) in lungs in combination with less pronounced thrombotic, inflammatory, and other pathological alterations in heart, brain, and kidneys.

ACKNOWLEDGEMENTS

We thank Dr. Ivan S. Raginov for the administrative support and Dr. Vladimir A. Anokhin for helpful discussions. Transmission electron microscopy was carried out in the Interdisciplinary Center for Analytical Microscopy of Kazan Federal University.

CONFLICT OF INTEREST

Authors declare that they have no competing financial interests in relation to the work.

AUTHOR CONTRIBUTION

J. W. Weisel and R. I. Litvinov performed study concept and design; R. R. Khismatullin, K. T. Montone, J. W. Weisel, and R. I. Litvinov performed development of methodology and writing, review and revision of the paper; R. R. Khismatullin, A. A. Ponomareva, C. Nagaswami, and R. A. Ivaeva provided acquisition, analysis and interpretation of data, and statistical analysis. All authors read and approved the final paper.

ORCID

John W. Weisel  <https://orcid.org/0000-0002-9628-257X>

Rustem I. Litvinov  <https://orcid.org/0000-0003-0643-1496>

REFERENCES

- Ruan Q, Yang K, Wang W, Jiang L, Song J. Clinical predictors of mortality due to COVID-19 based on an analysis of data of 150 patients from Wuhan, China. *Intensive Care Med.* 2020;46:846-848. doi:10.1007/s00134-020-05991-x
- Zhu N, Zhang D, Wang W, et al. A novel coronavirus from patients with pneumonia in China, 2019. *N Engl J Med.* 2020;82:727-733. doi:10.1056/NEJMoa2001017
- Wu Z, McGoogan JM. Characteristics of and important lessons from the coronavirus disease 2019 (COVID-19) outbreak in China: summary of a report of 72 314 cases from the Chinese center for disease control and prevention. *JAMA.* 2020;323:1239-1242. doi:10.1001/jama.2020.2648
- Zhou P, Yang XL, Wang XG, et al. A pneumonia outbreak associated with a new coronavirus of probable bat origin. *Nature.* 2020;579:270-273. doi:10.1038/s41586-020-2012-7
- Lai CC, Shih TP, Ko WC, Tang HJ, Hsueh PR. Severe acute respiratory syndrome coronavirus 2 (SARS-CoV-2) and coronavirus disease-2019 (COVID-19): the epidemic and the challenges. *Int J Antimicrob Agents.* 2020;55:105924. doi:10.1016/j.ijantimicag.2020.105924
- Guo T, Fan Y, Chen M, et al. Cardiovascular implications of fatal outcomes of patients with coronavirus disease 2019 (COVID-19). *JAMA Cardiol.* 2020;5:811-818. doi:10.1001/jamacardio.2020.1017
- Shi S, Qin M, Shen B, et al. Association of cardiac injury with mortality in hospitalized patients with COVID-19 in Wuhan, China. *JAMA Cardiol.* 2020;5:802-810. doi:10.1001/jamacardio.2020.0950
- Cheng Y, Luo R, Wang K, et al. Kidney disease is associated with in-hospital death of patients with COVID-19. *Kidney Int.* 2020;97:829-838. doi:10.1016/j.kint.2020.03.005
- Tang N, Bai H, Chen X, Gong J, Li D, Sun Z. Anticoagulant treatment is associated with decreased mortality in severe coronavirus disease 2019 patients with coagulopathy. *J Thromb Haemost.* 2020;18:1094-1099. doi:10.1111/jth.14817
- Thachil J, Tang N, Gando S, et al. ISTH interim guidance on recognition and management of coagulopathy in COVID-19. *J Thromb Haemost.* 2020;18:1023-1026. doi:10.1111/jth.14810
- Thachil J, Srivastava A. SARS-2 coronavirus-associated hemostatic lung abnormality in COVID-19: is it pulmonary thrombosis or pulmonary embolism? *Semin Thromb Hemost.* 2020;46:777-780. doi:10.1055/s-0040-1712155
- Fox SE, Akmatbekov A, Harbert JL, Li G, Quincy Brown J, Vander Heide RS. Pulmonary and cardiac pathology in African American patients with COVID-19: an autopsy series from New Orleans. *Lancet Respir Med.* 2020;8:681-686. doi:10.1016/S2213-2600(20)30243-5
- Becker RC. COVID-19 update: Covid-19-associated coagulopathy. *J Thromb Thrombolysis.* 2020;50:54-67. doi:10.1007/s11239-020-02134-3
- Zhou F, Yu T, Du R, et al. Clinical course and risk factors for mortality of adult inpatients with COVID-19 in Wuhan, China: a retrospective cohort study. *Lancet.* 2020;395:1054-1062. doi:10.1016/S0140-6736(20)30566-3
- Engelmann B, Massberg S. Thrombosis as an intravascular effector of innate immunity. *Nat Rev Immunol.* 2013;13:34-45. doi:10.1038/nri3345
- Temporary guidelines "Prevention, diagnosis and treatment of the new coronavirus infection (COVID-19)". Ministry of Health of the Russian Federation. Version 10. 08.02.2021. 261 p. (In Russ.)

17. Khismatullin RR, Shakirova AZ, Weisel JW, Litvinov RI. Age-dependent differential staining of fibrin in blood clots and thrombi. *BioNanoScience*. 2020;10:370-374. doi:10.1007/s12668-019-00701-4
18. Cardinal-Fernández P, Lorente JA, Ballén-Barragán A, Matute-Bello G. Acute respiratory distress syndrome and diffuse alveolar damage. New insights on a complex relationship. *Ann Am Thorac Soc*. 2017;14:844-850. doi:10.1513/AnnalsATS.201609-728PS
19. Cocucci E, Meldolesi J. Ectosomes and exosomes: shedding the confusion between extracellular vesicles. *Trends Cell Biol*. 2015;25:364-372. doi:10.1016/j.tcb.2015.01.004
20. Sheng ZM, Chertow DS, Ambroggio X, et al. Autopsy series of 68 cases dying before and during the 1918 influenza pandemic peak. *Proc Natl Acad Sci USA*. 2011;108:16416-16421. doi:10.1073/pnas.1111179108
21. Zhang H, Zhou P, Wei Y, et al. Histopathologic changes and SARS-CoV-2 immunostaining in the lung of a patient with COVID-19. *Ann Intern Med*. 2020;172:629-632. doi:10.7326/M20-0533
22. Puelles VG, Lütgehetmann M, Lindenmeyer MT, et al. Multiorgan and renal tropism of SARS-CoV-2. *N Engl J Med*. 2020;383:590-592. doi:10.1056/NEJMc2011400
23. Inciardi RM, Lupi L, Zaccone G, et al. Cardiac involvement in a patient with coronavirus disease 2019 (COVID-19). *JAMA Cardiol*. 2020;5:819-824. doi:10.1001/jamacardio.2020.1096
24. Monteil V, Kwon H, Prado P, et al. Inhibition of SARS-CoV-2 infections in engineered human tissues using clinical-grade soluble human ACE2. *Cell*. 2020;181:905-913.e7. doi:10.1016/j.cell.2020.04.004
25. Bonetti PO, Lerman LO, Lerman A. Endothelial dysfunction: a marker of atherosclerotic risk. *Arterioscler Thromb Vasc Biol*. 2003;23:168-175. doi:10.1161/01.ATV.0000051384.43104.FC
26. Edler C, Schröder AS, Aepfelbacher M, et al. Dying with SARS-CoV-2 infection-an autopsy study of the first consecutive 80 cases in Hamburg, Germany. *Int J Legal Med*. 2020;134:1275-1284. doi:10.1007/s00414-020-02317-w
27. Wichmann D, Sperhake JP, Lütgehetmann M, et al. Autopsy findings and venous thromboembolism in patients with COVID-19: a prospective cohort study. *Ann Intern Med*. 2020;173:268-277. doi:10.7326/M20-2003
28. Corbett V, Hassouna H, Girgis R. *In situ* thrombosis of the pulmonary arteries: an emerging new perspective on pulmonary embolism. *Med Student Res J*. 2015;4:54-58.
29. Páramo JA. Pulmonary embolism, pulmonary microvascular thrombosis, or both in COVID-19? *Clin Appl Thromb Hemost*. 2020;26:1076029620933953. doi:10.1177/1076029620933953
30. Xu Z, Shi L, Wang Y, et al. Pathological findings of COVID-19 associated with acute respiratory distress syndrome. *Lancet Respir Med*. 2020;8:420-422. doi:10.1016/S2213-2600(20)30076-X
31. Klok FA, Kruip MJHA, van der Meer NJM, et al. Incidence of thrombotic complications in critically ill ICU patients with COVID-19. *Thromb Res*. 2020;191:145-147. doi:10.1016/j.thromres.2020.04.013
32. Llitjos JF, Leclerc M, Chochois C, et al. High incidence of venous thromboembolic events in anticoagulated severe COVID-19 patients. *J Thromb Haemost*. 2020;18:1743-1746. doi:10.1111/jth.14869
33. Léonard-Lorant I, Delabranche X, Séverac F, et al. Acute pulmonary embolism in patients with COVID-19 at CT angiography and relationship to d-dimer levels. *Radiology*. 2020;296:E189-E191.
34. Chernysh IN, Nagaswami C, Kosolapova S, et al. The distinctive structure and composition of arterial and venous thrombi and pulmonary emboli. *Sci Rep*. 2020;10:5112. doi:10.1038/s41598-020-59526-x
35. Berry GJ & Rouse RV Acute interstitial pneumonia - diffuse alveolar damage. Online source: <https://surgepathcriteria.stanford.edu/lung/acute-interstitial-pneumonia-diffuse-alveolar-damage/>. Accessed November 20, 2010.
36. Krautgartner WD, Klappacher M, Hannig M, et al. Fibrin mimics neutrophil extracellular traps in SEM. *Ultrastruct Pathol*. 2010;34:226-231. doi:10.3109/01913121003725721
37. Perdomo J, Leung HHL, Ahmadi Z, et al. Neutrophil activation and NETosis are the major drivers of thrombosis in heparin-induced thrombocytopenia. *Nat Commun*. 2019;10:1322. doi:10.1038/s41467-019-09160-7
38. Middleton EA, He XY, Denorme F, et al. Neutrophil extracellular traps contribute to immunothrombosis in COVID-19 acute respiratory distress syndrome. *Blood*. 2020;136:1169-1179. doi:10.1182/blood.2020007008
39. Massberg S, Grahl L, von Bruehl ML, et al. Reciprocal coupling of coagulation and innate immunity via neutrophil serine proteases. *Nat Med*. 2010;16:887-896. doi:10.1038/nm.2184
40. Clark SR, Ma AC, Tavener SA, et al. Platelet TLR4 activates neutrophil extracellular traps to ensnare bacteria in septic blood. *Nat Med*. 2007;13:463-469. doi:10.1038/nm1565
41. Nicolai L, Gaertner F, Massberg S. Platelets in host defense: experimental and clinical insights. *Trends Immunol*. 2019;40:922-938. doi:10.1016/j.it.2019.08.004
42. Grobler C, Maphumulo SC, Grobbelaar LM, et al. Covid-19: the rollercoaster of fibrin(ogen), d-dimer, von Willebrand factor, p-selectin and their interactions with endothelial cells, platelets and erythrocytes. *Int J Mol Sci*. 2020;21:5168. doi:10.3390/ijms21145168
43. Veras FP, Pontelli MC, Silva CM, et al. SARS-CoV-2-triggered neutrophil extracellular traps mediate COVID-19 pathology. *J Exp Med*. 2020;217:e20201129. doi:10.1084/jem.20201129
44. Gollomp K, Sarkar A, Harikumar S, et al. Fc-modified HIT-like monoclonal antibody as a novel treatment for sepsis. *Blood*. 2020;135:743-754. doi:10.1182/blood.2019002329
45. Dittmayer C, Meinhardt J, Radbruch H, et al. Why misinterpretation of electron micrographs in SARS-CoV-2-infected tissue goes viral. *Lancet*. 2020;396:e64-e65. doi:10.1016/S0140-6736(20)32079-1
46. Bradley BT, Maioli H, Johnston R, et al. Histopathology and ultrastructural findings of fatal COVID-19 infections in Washington State: a case series. *Lancet*. 2020;396:320-332. doi:10.1016/S0140-6736(20)31305-2
47. Su H, Yang M, Wan C, et al. Renal histopathological analysis of 26 postmortem findings of patients with COVID-19 in China. *Kidney Int*. 2020;98:219-227. doi:10.1016/j.kint.2020.04.003
48. Martines RB, Ritter JM, Matkovic E, et al. Pathology and pathogenesis of SARS-CoV-2 associated with fatal coronavirus disease, United States. *Emerg Infect Dis*. 2020;26:2005-2015. doi:10.3201/eid2609.202095
49. Bullock HA, Goldsmith CS, Miller SE. Best practices for correctly identifying coronavirus by transmission electron microscopy. *Kidney Int*. 2021;99:824-827. doi:10.1016/j.kint.2021.01.004
50. Zhao CL, Rapkiewicz A, Maghsoodi-Deerwester M, et al. Pathological findings in the postmortem liver of patients with coronavirus disease 2019 (COVID-19). *Hum Pathol*. 2020;109:59-68. doi:10.1016/j.humpath.2020.11.015
51. Nicolai L, Leunig A, Brambs S, et al. Immunothrombotic dysregulation in COVID-19 pneumonia is associated with respiratory failure and coagulopathy. *Circulation*. 2020;142:1176-1189. doi:10.1161/CIRCULATIONAHA.120.048488

How to cite this article: Khismatullin RR, Ponomareva AA, Nagaswami C, et al. Pathology of lung-specific thrombosis and inflammation in COVID-19. *J Thromb Haemost*. 2021;19:3062-3072. doi:[10.1111/jth.15532](https://doi.org/10.1111/jth.15532)